We are IntechOpen,
the world's leading publisher of
Open Access books
Built by scientists, for scientists

4,800
Open access books available

122,000
International authors and editors

135M
Downloads

Our authors are among the

154
Countries delivered to

TOP 1%
most cited scientists

12.2%
Contributors from top 500 universities

CLARIVATE ANALYTICS
BOOK CITATION INDEX
INDEXED

WEB OF SCIENCE™

Selection of our books indexed in the Book Citation Index
in Web of Science™ Core Collection (BKCI)

Interested in publishing with us?
Contact book.department@intechopen.com

Numbers displayed above are based on latest data collected.
For more information visit www.intechopen.com

Modeling and Control of a Smart Single-Layer Graphene Sheet

A. Ghorbanpour Arani and F. Ebrahimi

Additional information is available at the end of the chapter

Abstract

In this study, a smart single-layer graphene sheet (SLGS) is analytically modeled and its buckling is controlled using coupled polyvinylidene fluoride (PVDF) nanoplates. A voltage is applied to the PVDF nanoplate in thickness direction in order to control the critical load of the SLGS. Electric potential distribution is assumed as a combination of a half-cosine and linear variation in order to satisfy the Maxwell equation. The exact analysis is performed for the case when all four ends are simply supported and in free electrical boundary condition. The nonlocal governing equations are derived through Hamilton's principle and energy method based on a nonlocal Mindlin plate theory. The detailed mathematical derivations are presented and numerical investigations are performed, while the emphasis is placed on investigating the effect of several parameters such as small-scale coefficient, stiffness of the internal elastic medium, graphene length, mode number, and external electric voltage on the buckling smart control of the SLGS in detail. It is explicitly shown that the imposed external voltage is an effective controlling parameter for buckling of the SLGS. Numerical results are presented to serve as benchmarks for design and smart control of nanodevices.

Keywords: Smart control, Mindlin plate theory, buckling analysis, coupled system, Pasternak model

1. Introduction

In recent years, nanostructural carbon materials have received considerable interest from the scientific community due to their superior properties. Among carbon-based nanomaterials, single-layered graphene sheet (SLGS) is defined as a flat monolayer of carbon atoms tightly packed into a two-dimensional honeycomb lattice, in which carbon atoms bond covalently with their neighbors [1,2]. Graphene sheets (GSs) possess extraordinary properties, such as

INTECH
open science | open minds

strong mechanical strength (Young's modulus = 1.0 TPa), large thermal conductivity (thermal conductivity = 3000 W/Km), excellent electric conductivity (electric conductivity up to 6000 S/cm), high surface area, and unusual optical properties [3-5]. These unique properties have made GSs one of the most promising materials in many applications such as nanosensors, nano-electronics, nanocomposites, batteries, nano-oscillators, nano-actuators, nanoresonators, nano-optomechanical systems, supercapacitors, fuel cells, solar cells, and hydrogen storage [6, 7]. On the other hand, polyvinylidene fluoride (PVDF) is a piezoelectric polymer. It has superior properties, such as excellent dimensional stability, abrasion and corrosion resistance, high strength, and capability of maintaining its mechanical properties at elevated temperature [8]. In contrast to GS, PVDF is a smart material, since it has piezoelectric property. The specific characteristic of piezoelectric materials is their ability to produce an electric field when deformed, and undergo deformation when subjected to an electric field. The coupling nature of piezoelectric materials has wide applications in electromechanical and electric devices, such as electromechanical actuators, sensors, and transducers [9].

Understanding mechanical behaviors of GSs is a key step for designing many nano-electro-mechanical system (NEMS) devices. Especially, stability response of GSs as NEMS component has great importance. Many studies have been carried out on the basis of nonlocal elasticity theory, which was initiated in the papers of Eringen [10-12]. He regarded the stress state at a given point as a function of the strain states of all points in the body, while the local continuum mechanics assumes that the stress state at a given point depends uniquely on the strain state at the same point. Pradhan and Murmu [13] studied small-scale effect on the buckling analysis of SLGS embedded in an elastic medium based on nonlocal plate theory. They found that the buckling loads of SLGS are strongly dependent on the small-scale coefficients and the stiffness of the surrounding elastic medium. Explicit analytical expressions for the critical buckling stresses in a monolayer GS based on nonlocal elasticity were investigated by Ansari and Rouhi [14]. They concluded that with the appropriate selection of the nonlocal parameter, the nonlocal relations are capable of yielding excellent results from the static deflection of monolayer GS under a uniformly distributed load. Also, their results showed that the importance of the small length scale is dependent on the boundary conditions of monolayer GS. Akhavan et al. [15] introduced exact solutions for the buckling analysis of rectangular Mindlin plates subjected to uniformly and linearly distributed in-plane loading on two opposite edges simply supported resting on elastic foundation. Their results indicated that the buckling load parameter increases as the thickness-to-length ratio decreases. Hashemi and Samaei [16] proposed an analytical solution for the buckling analysis of rectangular nanoplates based on the nonlocal Mindlin plate theory. They graphically presented the effects of small length scale on buckling loads for different geometrical parameters.

Samaei et al. [17] employed nonlocal Mindlin plate theory to analyze buckling of SLGS embedded in an elastic medium. They found that the effects of small length scale and surrounding elastic medium are significant to the mechanical behavior of nanoplates or SLGS and cannot be ignored. Furthermore, they showed that the nonlocal assumptions present larger buckling loads and stiffness of elastic medium in comparison to classical plate theory.

With respect to developmental works on mechanical behavior analysis of SLGS, it should be noted that none of the research mentioned above [13-17] have considered coupled double-

nanoplate system. Herein, Murmu and Adhikari [18] analyzed nonlocal vibration of bonded double-nanoplate systems. Their study highlighted that the small-scale effects considerably influence the transverse vibration of NDNPS. Besides, they elucidated that the increase of the stiffness of the coupling springs in nonlocal double-nanoplate system (NDNPS) reduces the small-scale effects during the asynchronous modes of vibration. Also, nonlocal buckling behavior of bonded double-nanoplate system was studied by Murmu et al. [19] who showed that the nonlocal effects in coupled system are higher with increasing values of the nonlocal parameter for the case of synchronous buckling modes than in the asynchronous buckling modes. Moreover, their analytical results indicated that the increase of the stiffness of the coupling springs in the double-GS system reduces the nonlocal effects during the asynchronous modes of buckling. Both papers [18, 19] have considered Winkler model for simulation of elastic medium between two nanoplates. In this simplified model, a proportional interaction between pressure and deflection of SLGSs is assumed, which is carried out in the form of discrete and independent vertical springs. Whereas, Pasternak suggested considering not only the normal stresses but also the transverse shear deformation and continuity among the spring elements, and its subsequent applications for developing the model for buckling analysis proved to be more accurate than the Winkler model. To the best of our knowledge, none of works in the literature have taken into account the Pasternak model for coupled system. This study aims to couple SLGS with PVDF nanoplate by an elastic medium which is simulated by the Pasternak model.

The use of smart materials has received considerable attention due to their higher potential applicability for the mechanical behavior control in various research areas. These materials can produce control forces to structural elements according to the applied voltage. A number of researchers utilized the piezoelectric materials to control mechanical behavior. For example, analysis of composite plates with piezoelectric actuators for vibration controls using layerwise displacement theory was performed by Han and Lee [20]. Piezoelectric control of composite plate vibration was carried out by Pietrzakowski [21], who considered effect of electric potential distribution. Recently, Liao et al. [22] examined nonlinear vibration of the piezoelectric nanobeams based on the nonlocal theory by considering external voltage. They assumed an electric potential as a combination of cosine and linear variation. They observed that the positive/negative voltage decreases/increases the linear and nonlinear frequencies of the nanobeam. None of the aforementioned studies [20-22] have considered a nanostructure (e.g., SLGS) whose vibrational behavior is controlled by an elastically bonded smart material (e.g., PVDF nanoplate).

However, to date, no report has been found in the literature on buckling analysis and smart control of SLGS using elastically coupled PVDF nanoplate based on nonlocal Mindlin plate theory. Motivated by these considerations, in order to improve optimum design of nanostructures, we aim to investigate the buckling smart control of SLGS based on nonlocal Mindlin plate theory. Herein, SLGS is elastically coupled with PVDF nanoplate and controlled by applying external electric voltage in thickness direction of PVDF nanoplate. The influences of external electric voltage, small-scale parameter, elastic medium, length of SLGS, and axial half wave number on buckling behavior of SLGS have been taken into account.

2. Review of nonlocal piezoelasticity and Mindlin plate theory

2.1. Nonlocal piezoelasticity

Based on the theory of nonlocal piezoelasticity, the stress tensor and the electric displacement at a reference point depend not only on the strain components and electric-field components at same position but also on all other points of the body. The nonlocal constitutive behavior for the piezoelectric material can be given as follows [22]:

$$\sigma_{ij}^{nl}(x) = \int_{v} \alpha(|x - x'|, \tau)\sigma_{ij}^{l} dV(x'), \qquad \forall x \in V \tag{1}$$

$$D_{k}^{nl} = \int_{v} \alpha(|x - x'|, \tau)D_{k}^{l} dV(x'), \qquad \forall x \in V \tag{2}$$

where σ_{ij}^{nl} and σ_{ij}^{l} are, respectively, the nonlocal stress tensor and local stress tensor; D_{k}^{nl} and D_{k}^{l} are the components of the nonlocal and local electric displacement; $\alpha(|x - x'|, \tau)$ is the nonlocal modulus; $|x - x'|$ is the Euclidean distance; and $\tau = e_0 a / l$ is defined such that l is the external characteristic length, e_0 denotes constant appropriate to each material, and a is the internal characteristic length of the material. Consequently, $e_0 a$ is a constant parameter which is obtained with molecular dynamics, experimental results, experimental studies, and molecular structure mechanics. The constitutive equation of the nonlocal elasticity can be written as [20]:

$$(1 - \mu\nabla^2)\sigma_{ij}^{nl} = \sigma_{ij}^{l}, \tag{3}$$

where the parameter $\mu = (e_0 a)^2$ denotes the small-scale effect on the response of structures in nanosize, and ∇^2 is the Laplacian operator in the above equation. Similarly, Eq. (2) can be written as [22]:

$$(1 - \mu\nabla^2)D_{k}^{nl} = D_{k}^{l}. \tag{4}$$

2.2. Mindlin plate theory

Based on the Mindlin plate theory, the displacement field can be expressed as [15-17]:

$$\begin{aligned}
u_x(x, y, z, t) &= z\psi_x(x, y, t), \\
u_y(x, y, z, t) &= z\psi_y(x, y, t), \\
u_z(x, y, z, t) &= w(x, y, t),
\end{aligned} \tag{5}$$

where $\psi_x(x, y)$ and $\psi_y(x, y)$ are the rotations of the normal to the mid-plane about x- and y-directions, respectively.

The von Kármán strains associated with the above displacement field can be expressed in the following form:

$$\varepsilon_{xx} = z\frac{\partial \psi_x}{\partial x}, \varepsilon_{yy} = z\frac{\partial \psi_y}{\partial y}, \gamma_{yz} = \frac{\partial w}{\partial y} + \psi_y, \gamma_{xz} = \frac{\partial w}{\partial x} + \psi_x, \gamma_{xy} = z(\frac{\partial \psi_x}{\partial y} + \frac{\partial \psi_y}{\partial x}), \tag{6}$$

where $(\varepsilon_{xx}, \varepsilon_{yy})$ are the normal strain components and $(\gamma_{yz}, \gamma_{xz}, \gamma_{xy})$ are the shear strain components.

3. Modeling of the problem

Consider a coupled SLGS–PVDF nanoplate system as depicted in Fig. 1, in which geometrical parameters of length L, width b, and thickness h are indicated. The SLGS and PVDF nanoplate are coupled by an elastic medium which is simulated by Pasternak foundation. As is well-known, this foundation model is capable of both transverse shear loads (k_g) and normal loads (k_w). The PVDF nanoplate is subjected to external electric voltage ϕ in thickness direction which is used for buckling smart control of SLGS.
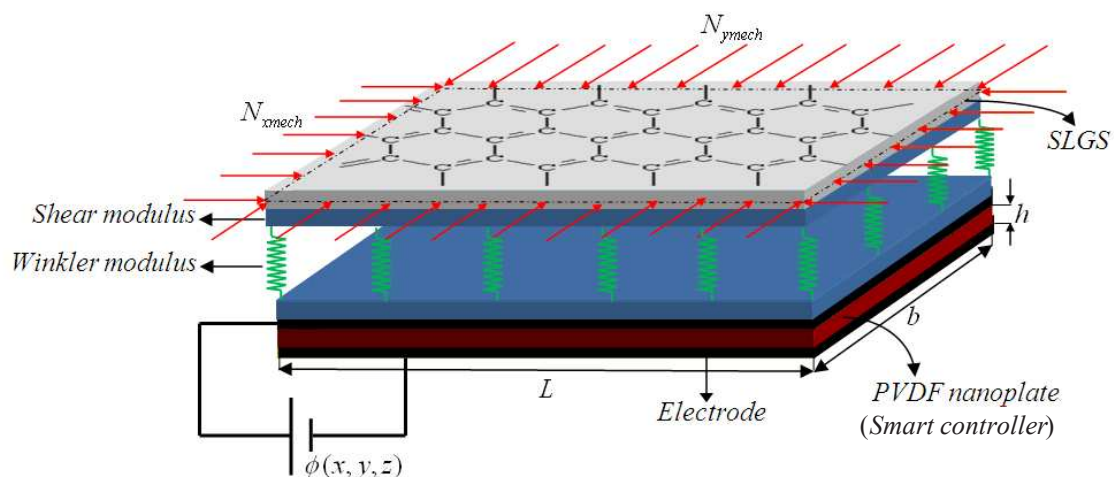
Figure 1. SLGS coupled by a Pasternak foundation with PVDF nanoplate subjected to applied external electric potential in thickness direction.

3.1. Constitutive relations for PVDF nanoplate

In a piezoelectric material, application of an electric field will cause a strain proportional to the mechanical field strength, and vice versa. The constitutive equation for stresses σ and

strains ε matrix on the mechanical side, as well as flux density D and field strength E matrix on the electrostatic side, may be arbitrarily combined as follows [23]:

$$\begin{Bmatrix} \sigma_{xx} \\ \sigma_{yy} \\ \sigma_{yz} \\ \sigma_{zx} \\ \sigma_{xy} \end{Bmatrix} = \begin{bmatrix} C_{11}^{PVDF} & C_{12}^{PVDF} & 0 & 0 & 0 \\ C_{21}^{PVDF} & C_{22}^{PVDF} & 0 & 0 & 0 \\ 0 & 0 & C_{44}^{PVDF} & 0 & 0 \\ 0 & 0 & 0 & C_{55}^{PVDF} & 0 \\ 0 & 0 & 0 & 0 & C_{66}^{PVDF} \end{bmatrix} \begin{Bmatrix} \varepsilon_{xx} \\ \varepsilon_{yy} \\ \gamma_{yz} \\ \gamma_{xz} \\ \gamma_{xy} \end{Bmatrix} - \begin{bmatrix} 0 & 0 & e_{31} \\ 0 & 0 & e_{32} \\ 0 & e_{24} & 0 \\ e_{15} & 0 & 0 \\ 0 & 0 & 0 \end{bmatrix} \begin{Bmatrix} E_{xx} \\ E_{yy} \\ E_{zz} \end{Bmatrix}, \quad (7)$$

$$\begin{Bmatrix} D_{xx} \\ D_{yy} \\ D_{zz} \end{Bmatrix} = \begin{bmatrix} 0 & 0 & 0 & e_{15} & 0 \\ 0 & 0 & e_{24} & 0 & 0 \\ e_{31} & e_{32} & 0 & 0 & 0 \end{bmatrix} \begin{Bmatrix} \varepsilon_{xx} \\ \varepsilon_{yy} \\ \gamma_{yz} \\ \gamma_{xz} \\ \gamma_{xy} \end{Bmatrix} + \begin{bmatrix} \in_{11} & 0 & 0 \\ 0 & \in_{22} & 0 \\ 0 & 0 & \in_{33} \end{bmatrix} \begin{Bmatrix} E_{xx} \\ E_{yy} \\ E_{zz} \end{Bmatrix}, \quad (8)$$

where C_{ij}^{PVDF}, e_{ij}, and $\in_{ij}$ denote elastic, piezoelectric, and dielectric coefficients, respectively. Also, electric field E_i ($i = x$, y, z) in terms of electric potential (ϕ) is given as follows [23]:

$$E = -\nabla \Phi. \quad (9)$$

The electric potential distribution in the thickness direction of the PVDF nanoplate in the form proposed by references [21] and [24] as the combination of a half-cosine and linear variation which satisfies the Maxwell equation is adopted as follows:

$$\Phi(x, y, z, t) = -\cos(\frac{\pi z}{h})\phi(x, y, t) + \frac{2zV_0}{h}e^{i\Omega t} \quad (10)$$

where $\phi(x, y, t)$ is the time and spatial distribution of the electric potential caused by bending which must satisfy the electric boundary conditions, V_0 is external electric voltage, and Ω is the natural frequency of the SLBNS which is zero for buckling analysis.

The strain energy of the PVDF nanoplate can be expressed as:

$$U = \frac{1}{2}\int_{\Omega_0}\int_{-h/2}^{h/2}\left(\sigma_{xx}\varepsilon_{xx} + \sigma_{yy}\varepsilon_{yy} + \sigma_{xy}\gamma_{xy} + \sigma_{xz}\gamma_{xz} + \sigma_{yz}\gamma_{yz} - D_{xx}E_{xx} - D_{yy}E_{yy} - D_{zz}E_{zz}\right) \quad (11)$$

Combining Eqs. (6)–(11) yields:

$$U = \frac{1}{2}\int_{\Omega_0}\left(M_{xx}\frac{\partial\psi_x}{\partial x} + M_{yy}\frac{\partial\psi_y}{\partial x} + M_{xy}\left(\frac{\partial\psi_x}{\partial y} + \frac{\partial\psi_y}{\partial x}\right) + Q_{xz}\left(\frac{\partial w_0}{\partial x} + \psi_x\right) + Q_{yz}\left(\frac{\partial w_0}{\partial y} + \psi_y\right)\right)dxdy$$
$$-\frac{1}{2}\int_{\Omega_0}\int_{-h/2}^{h/2}D_{xx}\left(\cos(\frac{\pi z}{h})\times\frac{\partial\phi}{\partial x}\right) + D_{yy}\left(\cos(\frac{\pi z}{h})\times\frac{\partial\varphi}{\partial x}\right) - D_{zz}\left(\frac{\pi}{h}\sin(\frac{\pi z}{h})\phi + \frac{2V_0}{h}\right)dzdxdy, \tag{12}$$

where the stress resultant-displacement relations can be written as:

$$\left\{(N_{xx},N_{yy},N_{xy}),(M_{xx},M_{yy},M_{xy})\right\} = \int_{-h/2}^{h/2}\left\{\sigma_{xx},\sigma_{yy},\tau_{xy}\right\}(1,z)dz, \tag{13}$$

$$\left\{Q_{xx},Q_{yy}\right\} = K\int_{-h/2}^{h/2}\left\{\tau_{xz},\tau_{yz}\right\}dz, \tag{14}$$

in which K is shear correction coefficient.

The external work due to surrounding elastic medium can be written as:

$$W = \frac{1}{2}\int_0^L q w_2 dx, \tag{15}$$

where q is related to Pasternak foundation. Finally, using Hamilton's principles lead to the following governing equations:

$$\frac{\partial M_{xx}^{PVDF}}{\partial x} + \frac{\partial M_{xy}^{PVDF}}{\partial y} - Q_{xx}^{PVDF} = 0, \tag{16}$$

$$\frac{\partial M_{xy}^{PVDF}}{\partial x} + \frac{\partial M_{yy}^{PVDF}}{\partial y} - Q_{yy}^{PVDF} = 0, \tag{17}$$

$$\frac{\partial Q_{xx}^{PVDF}}{\partial x} + \frac{\partial Q_{yy}^{PVDF}}{\partial y} - \left(1 - \mu\nabla^2\right)\left[k_w\left(w_1 - w_2\right) - k_g\nabla^2\left(w_1 - w_2\right) + (N_{xm} + N_{xe})\frac{\partial^2 w}{\partial x^2} + (N_{ym})\frac{\partial^2 w}{\partial y^2} = 0\right], \tag{18}$$

$$\int_{-h/2}^{h/2}\left[\cos(\frac{\pi z}{h})\frac{\partial D_{xx}}{\partial x} + \cos(\frac{\pi z}{h})\frac{\partial D_{yy}}{\partial x} + \frac{\pi}{h}\sin(\frac{\pi z}{h})D_{zz}\right]dz = 0, \tag{19}$$

in which k_w and k_g are Winkler and shear coefficients of Pasternak medium, respectively. Also, mechanical force are zero (i.e. $N_{xm} = N_{ym} = 0$) and electrical force is $N_{xe} = 2e_{11}V_0$. Substituting Eqs.

(7) and (8) into Eqs. (13) and (14), the stress resultant-displacement relations and electric displacement for PVDF nanoplate can be obtained as follows:

$$(1 - \mu\nabla^2)M_{xx}^{PVDF} = \frac{24he_{31}\phi + \pi h^3 C_{11}^{PVDF}\frac{\partial\psi_{xx}}{\partial x} + \pi h^3 C_{12}^{PVDF}\frac{\partial\psi_{yy}}{\partial y}}{12\pi}, \tag{20}$$

$$(1 - \mu\nabla^2)M_{yy}^{PVDF} = \frac{24he_{32}\phi + \pi h^3 C_{11}^{PVDF}\frac{\partial\psi_{yy}}{\partial y} + \pi h^3 C_{12}^{PVDF}\frac{\partial\psi_{xx}}{\partial x}}{12\pi}, \tag{21}$$

$$(1 - \mu\nabla^2)M_{xy}^{PVDF} = \frac{h^3 C_{66}^{PVDF}}{12}(\frac{\partial\psi_{xx}}{\partial y} + \frac{\partial\psi_{yy}}{\partial x}), \tag{22}$$

$$(1 - \mu\nabla^2)Q_{xx}^{PVDF} = \frac{Kh\left(-2e_{15}\frac{\partial\phi}{\partial x} + C_{55}^{PVDF}\pi(\psi_{xx} + \frac{\partial w}{\partial y})\right)}{\pi}, \tag{23}$$

$$(1 - \mu\nabla^2)Q_{yy}^{PVDF} = \frac{Kh\left(-2e_{24}\frac{\partial\phi}{\partial x} + C_{44}^{PVDF}\pi(\psi_{yy} + \frac{\partial w}{\partial y})\right)}{\pi}, \tag{24}$$

$$\int_{-h/2}^{h/2}\left[(1 - \mu\nabla^2)D_{xx}\right]\cos(\frac{\pi z}{h})\,dz = \left(\int_{-h/2}^{h/2}e_{15}\cos(\frac{\pi z}{h})dz\right)\left(\frac{\partial w}{\partial x} + \psi_{xx}\right) + \left(\int_{-h/2}^{h/2}\in_{11}\cos(\frac{\pi z}{h})^2\,dz\right)\frac{\partial\phi}{\partial x}, \tag{25}$$

$$\int_{-h/2}^{h/2}\left[(1 - \mu\nabla^2)D_{yy}\right]\cos(\frac{\pi z}{h})\,dz = \left(\int_{-h/2}^{h/2}e_{24}\cos(\frac{\pi z}{h})dz\right)\left(\frac{\partial w}{\partial y} + \psi_{yy}\right) + \left(\int_{-h/2}^{h/2}\in_{22}\cos(\frac{\pi z}{h})^2\,dz\right)\frac{\partial\phi}{\partial x}, \tag{26}$$

$$\int_{-h/2}^{h/2}\left[(1 - \mu\nabla^2)D_{zz}\right]\frac{\pi}{h}\sin(\frac{\pi z}{h})\,dz = \left(\int_{-h/2}^{h/2}e_{31}\frac{\pi}{h}\sin(\frac{\pi z}{h})zdz\right)\frac{\partial\psi_{xx}}{\partial x} + \left(\int_{-h/2}^{h/2}e_{32}\frac{\pi}{h}\sin(\frac{\pi z}{h})zdz\right)\frac{\partial\psi_{yy}}{\partial y}$$
$$- \left(\int_{-h/2}^{h/2}\in_{33}\left(\frac{\pi}{h}\sin(\frac{\pi z}{h})\right)^2\,dz\right)\phi. \tag{27}$$

3.2. Constitutive relations for SLGS

The SLGS is subjected to uniform compressive edge loading along x and y axis. In order to obtain the governing equations of SLGS, the procedure outlined above for PVDF nanoplate

can be expressed repeatedly by ignoring piezoelectric coefficient in Eq. (7) and electric displacement (Eq. (8)).

$$\frac{\partial M_{xx}^{GS}}{\partial x} + \frac{\partial M_{xy}^{GS}}{\partial y} - Q_{xx}^{GS} = 0,$$
(28)

$$\frac{\partial M_{xy}^{GS}}{\partial x} + \frac{\partial M_{yy}^{GS}}{\partial y} - Q_{yy}^{GS} = 0,$$
(29)

$$\frac{\partial Q_{xx}^{GS}}{\partial x} + \frac{\partial Q_{yy}^{GS}}{\partial y} - \left(1 - \mu\nabla^2\right)\left[k_w\left(w_2 - w_1\right) - k_g\nabla^2\left(w_2 - w_1\right) + (N_{xm})\frac{\partial^2 w}{\partial x^2} + (N_{ym})\frac{\partial^2 w}{\partial y^2} = 0\right].$$
(30)

It is noted that the superscript PVDF nanoplate in section 3.1 can be changed to *GS* in this section.

4. Solution procedure

Steady-state solutions to the governing equations of the plate motion and the electric potential distribution which relate to the simply supported boundary conditions and zero electric potential along the edges of the surface electrodes can be assumed as [17,21]:

$$\begin{Bmatrix} \psi_{x1}(x,y,t) \\ \psi_{y1}(x,y,t) \\ w_1(x,y,t) \\ \psi_{x2}(x,y,t) \\ \psi_{y2}(x,y,t) \\ w_2(x,y,t) \\ \phi_2(x,y,t) \end{Bmatrix} = \begin{Bmatrix} \bar{\psi}_{x1}\cos(\frac{m\pi x}{L})\sin(\frac{n\pi y}{b}) \\ \bar{\psi}_{y1}\sin(\frac{m\pi x}{L})\cos(\frac{n\pi y}{b}) \\ \bar{w}_1\sin(\frac{m\pi x}{L})\sin(\frac{n\pi y}{b}) \\ \bar{\psi}_{x2}\cos(\frac{m\pi x}{L})\sin(\frac{n\pi y}{b}) \\ \bar{\psi}_{y2}\sin(\frac{m\pi x}{L})\cos(\frac{n\pi y}{b}) \\ \bar{w}_2\sin(\frac{m\pi x}{L})\sin(\frac{n\pi y}{b}) \\ \bar{\phi}_2\sin(\frac{m\pi x}{L})\sin(\frac{n\pi y}{b}) \end{Bmatrix}.$$
(31)

As mentioned above, it is assumed that the SLGS plate is free from any transverse loadings. Uniform compressive edge loading along x and y axis are $N_{xm} = -P$ and $N_{ym} = -kP$, respectively. Substituting Eq. (31) into Eqs. (16)–(19) and (28)–(30) yields:

$$
\left\{
\begin{bmatrix}
L_{11} & L_{12} & L_{13} & L_{14} & 0 & 0 & 0 \\
L_{21} & L_{22} & L_{23} & 0 & 0 & 0 & 0 \\
L_{31} & L_{32} & L_{33} & 0 & 0 & 0 & 0 \\
L_{41} & 0 & 0 & L_{44} & L_{45} & L_{46} & L_{47} \\
0 & 0 & 0 & L_{54} & L_{55} & L_{56} & L_{57} \\
0 & 0 & 0 & L_{64} & L_{65} & L_{66} & L_{67} \\
0 & 0 & 0 & L_{74} & L_{75} & L_{76} & L_{77}
\end{bmatrix}
+ P\xi_{mn}\eta_{mn}
\begin{bmatrix}
1 & 0 & 0 & 0 & 0 & 0 & 0 \\
0 & 0 & 0 & 0 & 0 & 0 & 0 \\
0 & 0 & 0 & 0 & 0 & 0 & 0 \\
0 & 0 & 0 & 0 & 0 & 0 & 0 \\
0 & 0 & 0 & 0 & 0 & 0 & 0 \\
0 & 0 & 0 & 0 & 0 & 0 & 0 \\
0 & 0 & 0 & 0 & 0 & 0 & 0
\end{bmatrix}
\right\}
\begin{bmatrix}
\bar{w}_1 \\
\bar{\psi}_{x1} \\
\bar{\psi}_{y1} \\
\bar{w}_2 \\
\bar{\psi}_{x2} \\
\bar{\psi}_{y2} \\
\bar{\phi}_2
\end{bmatrix}
=
\begin{bmatrix}
0 \\
0 \\
0 \\
0 \\
0 \\
0 \\
0
\end{bmatrix}, \qquad (32)
$$

where $\xi_{mn} = 1 + \mu\left(\left(\dfrac{m\pi}{L}\right)^2 + \left(\dfrac{n\pi}{b}\right)^2\right)$, $\eta_{mn} = \left(\dfrac{m\pi}{L}\right)^2 + k\left(\dfrac{n\pi}{b}\right)^2$ and L_{ij} are defined in Appendix A. Finally, buckling load of the system (P) can be calculated by solving the above equation.

5. Numerical results

In this section, buckling smart control of SLGS using elastically bonded PVDF nanoplate is discussed so that the effects of nonlocal parameter, mode number, Pasternak foundation, and SLGS length on the buckling of the SLGS are also considered. For this purpose, buckling load ratio is defined as follows:

$$
\text{Buckling Load Ratio} = \frac{\text{Buckling load from nonlocal theory } (P_{nl})}{\text{Buckling load from local theory } (P_l)}
$$

The orthotropic mechanical properties of SLGS with thickness $h = 0.34$ nm are listed in Table 1 [25]. Also, mechanical and electrical characteristics of PVDF nanoplate with thickness $h = 2$ nm are presented in Table 1 [26], which are taken from the macroscopic piezoelectric materials. In fact, the polymeric piezoelectric nanomaterials' characteristics are size-dependent and determined by experiments or molecular dynamic (MD) simulation [22]. To the best of the author's knowledge, the experimental values of piezoelectric nanomaterials' properties are not available in the literature. Therefore, in order to quantitatively analyze the present work, the characteristics of PVDF nanoplate are assumed in macroscale.

The developed nonlocal theory to date is incapable of determining the small scaling parameter $e_0 a$. However, Eringen [11] proposed $e_0 a = 0.39$ nm by matching the dispersion curves using nonlocal theory for plane waves and Born–Karman model of lattice dynamics. For CNT, the

SLGS	PVDF
$E_1 = 1765 \, (GPa)$	$C_{11} = 238.24 \, (GPa)$
$E_2 = 1588 \, (GPa)$	$C_{22} = 23.60 \, (GPa)$
$v_{12} = 0.3$	$C_{12} = 3.98 \, (GPa)$
$v_{21} = 0.3$	$C_{44} = 2.15 \, (GPa)$
	$C_{55} = 4.40 \, (GPa)$
	$C_{66} = 6.43 \, (GPa)$
	$e_{31} = -0.13 \, (C/m^2)$
	$e_{32} = -0.145 \, (C/m^2)$
	$e_{24} = -0.276 \, (C/m^2)$
	$e_{15} = -0.009 \, (C/m^2)$
	$e_{32} = -0.145 \, (C/m^2)$
	$\in_{11} = 1.1068 \times 10^{-8} \, (F/m)$

Table 1. Material properties of PVDF and SLGS.

$e_0 a$ is found to be less than 2 nm [27]. Small-scale effects on the buckling behavior of SLGS and PVDF nanoplate were carried out analytically by assuming a range of values $0 < e_0 a < 2 \, nm$, since its exact value is not known [27].

In the absence of similar publications in the literature covering the same scope of the problem, one cannot directly validate the results found here. However, the present work could be partially validated based on a simplified analysis suggested by Samaei et al. [17], Pradhan [28], Murmu and Pradhan [29], and Hashemi and Samaei [16] on buckling of the SLGS for which the coupled PVDF nanoplate in this paper was ignored. For this purpose, an SLGS with $E = 1 \, TPa$, $v = 0.3$, $h = 0.34 \, nm$, and $5 < L < 50 \, nm$ [17] as well as a nanoplate with $E = 1765 \, GPa$, $v = 0.25$, $h = 0.34 \, nm$, and $5 < L < 50 \, nm$ [16] are considered.

On the same basis and assuming Mindlin plate theory for buckling of SLGS embedded in a Pasternak foundation, the results obtained here are compared with those of Samaei et al. [17]. The results are shown in Fig. 2, in which buckling load ratio versus nonlocal parameter is plotted for $K_g = 0$ and $K_g = 20$. It is noted that in this figure the shear modulus is normalized the same as [17], $K_g = k_g L^2 / D$ in which $D = Eh^3 / 12(1 - v^2)$. As can be seen, the two analyses agree well and show similar results. A comparison between the buckling analysis of SLGS using the theories of classical plate [29], higher-order shear deformation [28] and Mindlin plate [16] is presented in Table 2. In this table, critical buckling load for different values of nonlocal parameter and aspect ratio of length to thickness is shown. As can be seen, the present results based on Mindlin plate theory closely match with those reported by Hashemi and Samaei [16], Pradhan [28], and Murmu and Pradhan [29].
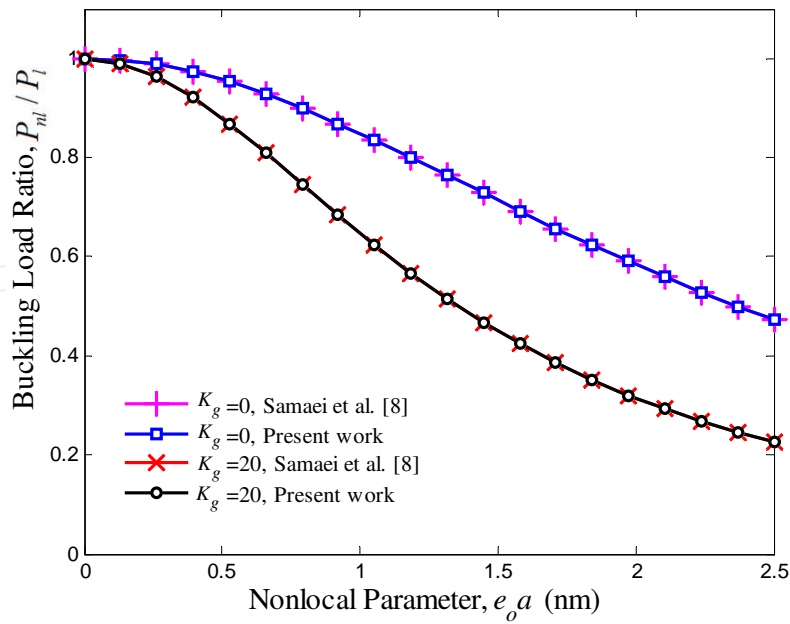
Figure 2. Comparison of buckling load ratio versus nonlocal parameter for $K_g = 0$ and $K_g = 20$.

L/h	μ	Dimensionless critical buckling load from higher order plate theory [28]	Dimensionless critical buckling load from classical plate theory [29]	Dimensionless critical buckling load from Mindlin plate theory (present work)	Dimensionless critical buckling load from Mindlin plate theory [16]
100	0.0	9.8791	9.8671	9.8671	9.8671
	0.5	9.4156	9.4031	9.4029	9.4028
	1.0	8.9947	8.9807	8.9803	8.9801
	1.5	8.6073	8.5947	8.5939	8.5939
	2.0	8.2537	8.2405	8.2393	8.2393
20	0.0	9.8177	9.8067	9.8067	9.8067
	0.5	9.3570	9.3455	9.3455	9.3451
	1.0	8.9652	8.9528	8.9527	8.9522
	1.5	8.5546	8.5421	8.5420	8.5419
	2.0	8.2114	8.1900	8.1898	8.1898

Table 2. Comparison between the buckling analysis of SLGS using the theories of classical plate, higher-order shear deformation and Mindlin plate.

The effect of the external electric voltage (V_0) on the buckling load ratio with respect to nonlocal parameter (μ) is demonstrated in Fig. 3. It is shown that applying positive electric potential can increase the buckling load ratio of the SLGS and vice versa. This is because the imposed positive and negative voltages generate the axial compressive and tensile forces in the PVDF nanoplate, respectively. Meanwhile, the effect of external voltage becomes more prominent at higher μ. Hence, the imposed external voltage is an effective controlling parameter for buckling of the SLGS which is coupled by a smart PVDF nanoplate. It is also concluded that increasing

the μ decreases the buckling load ratio. This is due to the fact that the increase of nonlocal parameter decreases the interaction force between graphene sheet atoms, and that leads to a softer structure. Figure 4 illustrates the effect of mode number of SLGS on the variation of buckling load ratio versus μ. As can be seen, buckling load ratio decreases with increasing mode numbers. Also, the small-scale effects on the buckling load ratio become more distinguished at higher modes. Obviously, the difference between the buckling load ratios of the SLGS is larger at higher nonlocal parameters. Furthermore, the buckling load ratio for all mode numbers decreases by increasing the μ.
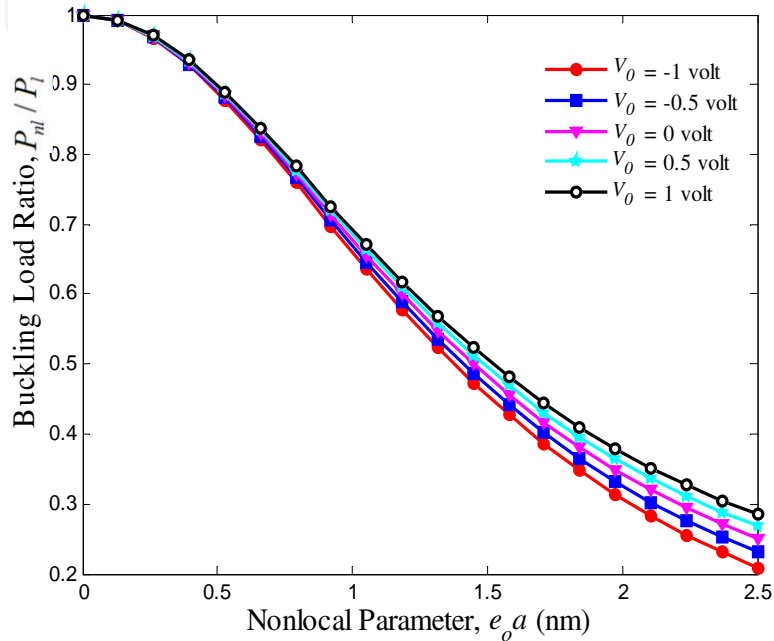

Figure 3. The effect of the external voltage on the buckling load ratio versus nonlocal parameter.
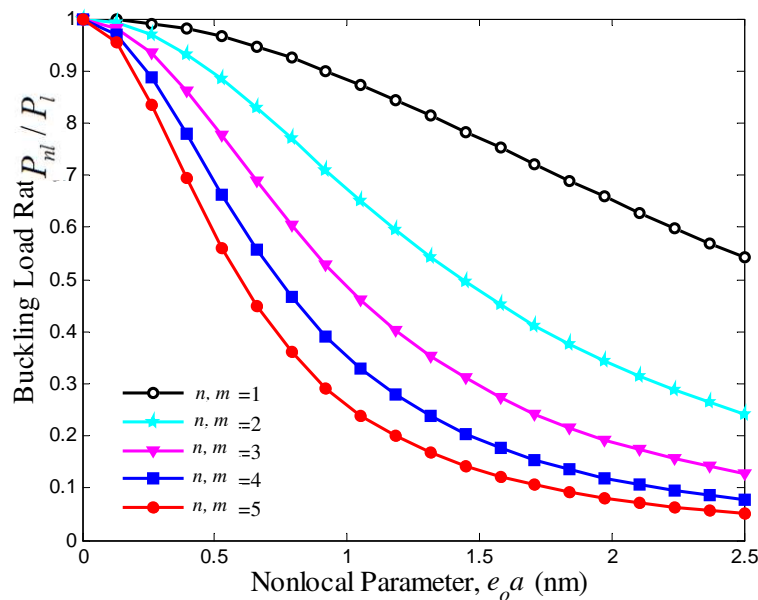

Figure 4. The effect of mode number on the buckling load ratio versus nonlocal parameter.

The effects of the SLGS length and the imposed external voltage to the PVDF nanoplate on the buckling load ratio are shown in Fig. 5. It is noted that the length of the SLGS is considered between $10 < L < 40$ nm, since the maximum length of the graphene sheet taken is 45.2896 nm in the literature by Sakhaee Pour [30], Pradhan and Murmu [13], and Samaei et al. [17]. As length of the graphene sheet increases, the buckling load ratio increases. It is also observed that for a given length, the SLGS, applying negative external voltage to PVDF nanoplate, will buckle first as compared to the SLGS with positive one.

Figure 6 depicts the effects of axial half wave number (m) and external voltage on the buckling load ratio of the SLGS. It is obvious that the buckling load ratio decreases sharply with increasing m. As can be seen, with the increase of external voltage, buckling load ratio is increased. Moreover, the effect of V_0 is not considerable for $m<2$. It means that the external voltage effect decreases with decrease of the axial half wave number.

Buckling smart control of SLGS using PVDF nanoplate versus shear modulus parameter (K_g) is plotted in Fig. 7. The obtained results show that at a given K_g, when the imposed external voltage changes from -1 V to 1 V, the buckling load ratio increases. It is also worth mentioning that the influences of V_0 at higher K_g values are more apparent than at lower K_g's. As the shear modulus parameter of the coupled system increases, generally, the buckling load ratio reduces and approaches a constant value. This is because increasing shear modulus parameter increases the structure stiffness.
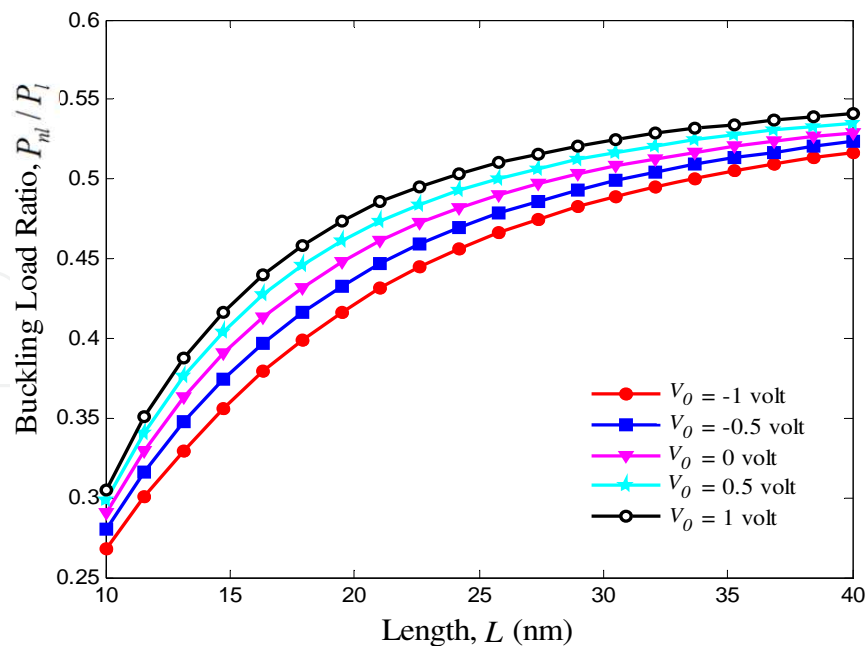

Figure 5. The effect of the external voltage on the buckling load ratio versus graphene length.
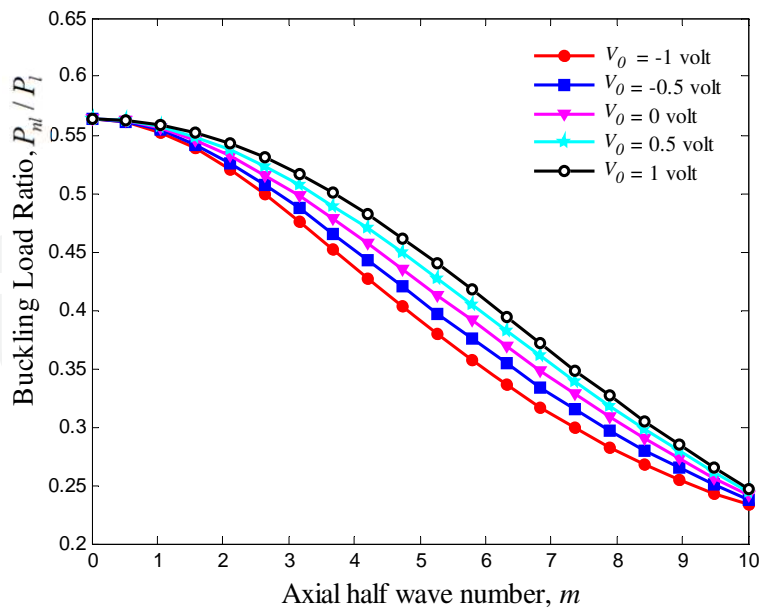
Figure 6. The effect of the external voltage on the buckling load ratio versus axial half wave number.
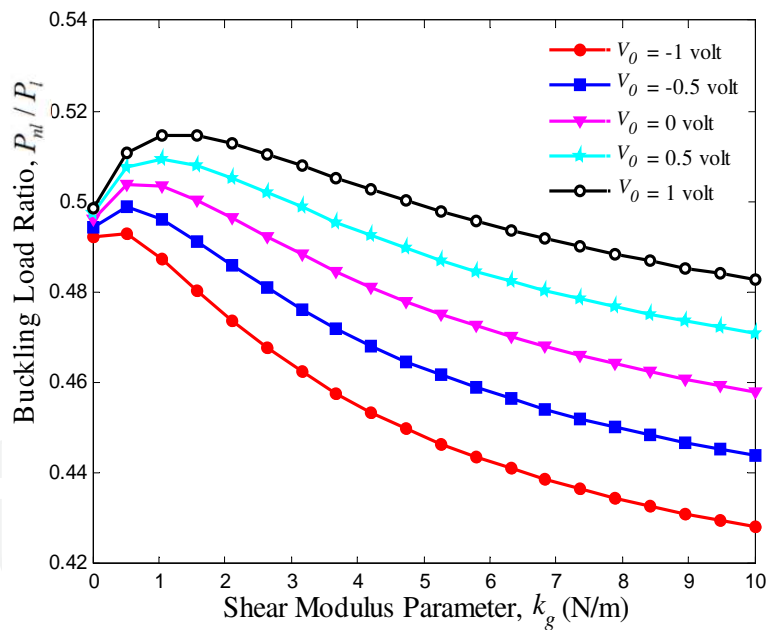

Figure 7. The effect of the external voltage on the buckling load ratio versus shear modulus parameter.

6. Conclusion

Buckling response of graphene sheets has applications in designing many NEMS/MEMS devices such as strain sensor, mass and pressure sensors, and atomic dust detectors. Buckling

smart control of the SLGS using elastically bonded PVDF nanoplate which is subjected to external voltage is the main contribution of the present paper. The elastic medium between SLGS and PVDF nanoplate is simulated by a Pasternak foundation. The governing equations are obtained based on nonlocal Mindlin plate theory so that the effects of small-scale, elastic medium coefficient, mode number, and graphene length are discussed. The results indicate that the imposed external voltage is an effective controlling parameter for buckling of the SLGS. It is found that the effect of external voltage becomes more prominent at higher nonlocal parameter and shear modulus. It is also observed that for a given length, the SLGS with negative external voltage will buckle first as compared to the SLGS with positive one. The results of this study are validated as far as possible by the buckling of SLGS in the absence of PVDF nanoplate, as presented by [16, 17, 28, and 29]. Finally, it is hoped that the results presented in this paper would be helpful for study and design of bonded systems based on smart control and electromechanical systems.

Appendix A

$$L_{11} = -\frac{KC_{55}^{GS}m^2\pi^2h}{L^2} - \frac{KC_{44}^{GS}n^2\pi^2h}{b^2} + k_w + k_g\left(\frac{m^2\pi^2}{L^2} + \frac{n^2\pi^2}{b^2}\right) -$$
$$\mu\left(-\frac{k_w m^2\pi^2}{L^2} - k_g\left(\frac{m^4\pi^4}{L^4} + \frac{m^2\pi^4 n^2}{L^2 b^2}\right) - \frac{k_w n^2\pi^2}{b^2} - k_g\left(\frac{m^2\pi^4 n^2}{L^2 b^2} + \frac{n^4\pi^4}{b^4}\right)\right)$$

$$L_{12} = -\frac{KC_{55}^{GS}m\pi h}{L}$$

$$L_{13} = -\frac{KC_{44}^{GS}n\pi h}{b}$$

$$L_{14} = -k_g\left(\frac{m^2\pi^2}{L^2} + \frac{n^2\pi^2}{b^2}\right) - k_w -$$
$$\mu\left(\frac{k_w m^2\pi^2}{L^2} + K_g\left(\frac{m^4\pi^4}{L^4} + \frac{m^4\pi^4 n^2}{L^2 b^2}\right) + \frac{k_w n^2\pi^2}{b^2} + k_g\left(\frac{m^2\pi^4 n^2}{L^2 b^2} + \frac{n^4\pi^4}{b^4}\right)\right)$$

$$L_{21} = -\frac{KC_{55}^{GS}m\pi h}{L}$$

$$L_{22} = -\frac{C_{11}^{GS}m^2\pi^2h^3}{12L^2} + \frac{C_{66}^{GS}n^2\pi^2h^3}{12b^2} + KC_{55}^{GS}h$$

$$L_{23} = -\frac{m\pi^2 n h^3}{12Lb}(C_{12}^{GS} + C_{66}^{GS})$$

$$L_{31} = -\frac{KC_{44}^{GS}n\pi h}{b}$$

$$L_{32} = -\frac{m\pi^2 n h^3}{12Lb}(C_{12}^{GS} + C_{66}^{GS})$$

$$L_{33} = -\frac{C_{66}^{GS} m^2 \pi^2 h^3}{12L^2} - \frac{C_{11}^{GS} n^2 \pi^2 h^3}{12b^2} - KC_{44}^{GS} h$$

$$L_{41} = -k_w - k_g \left(\frac{m^2\pi^2}{L^2} + \frac{n^2\pi^2}{b^2} \right) -$$

$$\mu \left(\left(\frac{k_w n^2 \pi^2}{b^2} + k_g \left(\frac{m^2\pi^4 n^2}{L^2 b^2} + \frac{n^4\pi^4}{b^4} \right) + \frac{k_w m^2 \pi^2}{L^2} + k_g \left(\frac{m^4\pi^4}{L^4} + \frac{m^2\pi^4 n^2}{L^2 b^2} \right) \right) \right)$$

$$L_{44} = -\frac{KC_{55}^{PVDF} m^2 \pi^2 h}{L^2} - \frac{KC_{44}^{PVDF} n^2 \pi^2 h}{b^2} - \frac{2e_{31}V_0 m^2 \pi^2}{L^2} + k_w + k_g \left(\frac{m^2\pi^2}{L^2} + \frac{n^2\pi^2}{b^2} \right) -$$

$$\mu \left(\frac{2e_{31}V_0 m^4 \pi^4}{L^4} - \frac{k_w m^2 \pi^2}{L^2} - k_g \left(\frac{m^4\pi^4}{L^4} + \frac{m^2\pi^4 n^2}{L^2 b^2} \right) + \frac{2e_{31}V_0 m^2 \pi^4 n^2}{L^2 b^2} - \frac{k_w n^2 \pi^2}{b^2} - k_g \left(\frac{m^2\pi^4 n^2}{L^2 b^2} + \frac{n^4\pi^4}{b^4} \right) \right)$$

$$L_{45} = -\frac{KC_{55}^{PVDF} m\pi h}{L}$$

$$L_{46} = -\frac{KC_{44}^{PVDF} n\pi h}{b}$$

$$L_{47} = \frac{2Khe_{15}m^2\pi}{L^2} + \frac{2Khe_{24}n^2\pi}{b^2}$$

$$L_{54} = -\frac{KC_{55}^{PVDF} m\pi h}{L}$$

$$L_{55} = -\frac{C_{11}^{PVDF} m^2 \pi^2 h^3}{12L^2} - \frac{C_{66}^{PVDF} n^2 \pi^2 h^3}{12b^2} - KC_{55}^{PVDF} h$$

$$L_{56} = -\frac{m\pi^2 n h^3}{12Lb}(C_{12}^{PVDF} + C_{66}^{PVDF})$$

$$L_{57} = \frac{2he_{31}m + 2Khe_{15}m}{L}$$

$$L_{64} = -\frac{KC_{44}^{PVDF} n\pi h}{b}$$

$$L_{65} = -\frac{m\pi^2 n h^3}{12Lb}(C_{12}^{PVDF} + C_{66}^{PVDF})$$

$$L_{66} = -\frac{C_{66}^{PVDF} m^2 \pi^2 h^3}{12L^2} - \frac{C_{11}^{PVDF} n^2 \pi^2 h^3}{12b^2} - KC_{44}^{PVDF} h \tag{33}$$

$$L_{67} = \frac{2he_{32}n}{b} + \frac{2Khe_{24}n}{b}$$

$$L_{74} = -\frac{4m^2 h^2 b^2 e_{15}\pi + 4n^2 h^2 L^2 e_{24}\pi}{2L^2 b^2 h}$$

$$L_{75} = -\frac{4m h^2 b^2 e_{15}L + 4Lb^2 e_{31}m h^2}{2L^2 b^2 h}$$

$$L_{76} = -\frac{4n h^2 L^2 e_{24}b + 4L^2 b e_{32}n h^2}{2L^2 b^2 h}$$

$$L_{77} = -\frac{h^2 m^2 \pi^2 \in_{11} b^2 + \in_{33} \pi^2 L^2 b^2 + h^2 n^2 \pi^2 \in_{22} L^2}{2L^2 b^2 h}$$

Author details

A. Ghorbanpour Arani[1] and F. Ebrahimi[2*]

*Address all correspondence to: febrahimy@eng.ikiu.ac.ir

1 Faculty of Mechanical Engineering, Institute of Nanoscience & Nanotechnology University of Kashan, Kashan, Islamic Republic of Iran

2 Department of Mechanical Engineering, Faculty of Engineering, Imam Khomeini International University, Qazvin, Islamic Republic of Iran

References

[1] M. Yang, A. Javadi, H. Li, Sh. Gong, *Biosens Bioelec*. 26 (2010) 560–565.

[2] B. Arash, Q. Wang, K.M. Liew, *Comput Meth Appl Mech Engin*. 223 (2012) 1–9.

[3] J.S. Oh, Ta. Hwang, G.Y. Nam, J.P. Hong, A.H. Bae, S.I. Son, G.H. Lee, H.k. Sung, H.R. Choi, J.C. Koo, J.D. Nam, *Thin Solid Film* (2011) In Press.

[4] C. Chen, W. Fu, C. Yu, *Mat Lett*. 82 (2012) 132–136.

[5] C. Baykasoglu, *Comput Mat Sci*. 55 (2012) 228–236.

[6] Y. Qian, C. Wang, Z.G. Le, *Appl Surf Sci*. 257 (2011) 10758–10762.

[7] E. Jomehzadeh, A.R. Saidi, *Comput Mat Sci*. 50 (2011) 1043–1051.

[8] A.A. Mosallaie Barzoki, A. Ghorbanpour Arani, R. Kolahchi, M.R. Mozdianfard, *Appl Math Model*. 36 (2012) 2983-2995.

[9] A. Ghorbanpour Arani, R. Kolahchi, A.A. Mosallaie Barzoki, A. Loghman, *Appl Math Model*. 36 (2012) 139–157.

[10] A.C. Eringen, *Int J Engin Sci*. 10 (1972) 1–16.

[11] A.C. Eringen, *J Appl Phys*. 54 (1983) 4703–4710.

[12] A.C. Eringen, *Nonlocal Continuum Field Theories*, Springer-Verlag, New York, 2002.

[13] S.C. Pradhan, T. Murmu, *Physica E*. 42 (2010) 1293–1301.

[14] R. Ansari, H. Rouhi, *Solid State Comm*. 152 (2012) 56–59.

[15] H. Akhavan, Sh. Hosseini Hashemi, H. Rokni Damavandi Taher, A. Alibeigloo, Sh. Vahabi, *Comput Mat Sci*. 44 (2009) 968–978.

[16] Sh. Hosseini Hashemi, A. Tourki Samaei, *Physica E*. 43 (2011) 1400–1404.

[17] A.T. Samaei, S. Abbasion, M.M. Mirsayar, *Mech Res Comm*. 38 (2011) 481– 485.

[18] T. Murmu, S. Adhikari, *Compos Part B: Engin*. 42 (2011) 1901–1911.

[19] T. Murmu, J. Sienz, J. Adhikari, C. Arnold, *J Appl Phys*. 110 (2011) 084316-9.

[20] J.H. Han, I. Lee, *Compos Part B: Engin 29B* (1998) 621–632.

[21] M. Pietrzakowski, *Comput Struct*. 86 (2008) 948–954

[22] L.L. Ke, Y.Sh. Wang, Zh.D. Wang, *Compos Struct*. 96 (2012) 2038–2047.

[23] A. Ghorbanpour Arani, R. Kolahchi, A.A. Mosallaie Barzoki, *Appl Math Model*. 35 (2011) 2771–2789.

[24] S.T. Quek, Q. Wang, *Smart Mater Struct*. 9 (2000) 859–867.

[25] S.C. Pradhan, A. Kumar, *Comput Mat Sci*. 50 (2010) 239–245.

[26] A. Salehi-Khojin, N. Jalili, *Compos Sci Technol*. 68 (2008) 1489–1501.

[27] Q. Wang, *J Appl Phys*. 98 (2005) 124301.

[28] S.C. Pradhan, *Phys Lett*. A 373 (2009) 4182–4188.

[29] S.C. Pradhan, T. Murmu, *Comput Mat Sci*. 47 (2009) 268–274.

[30] A. Sakhaee-Pour, Comput Mat Sci. 45 (2009) 266–270.